Reversible Cl₂/Cl⁻ redox for low-temperature aqueous batteries

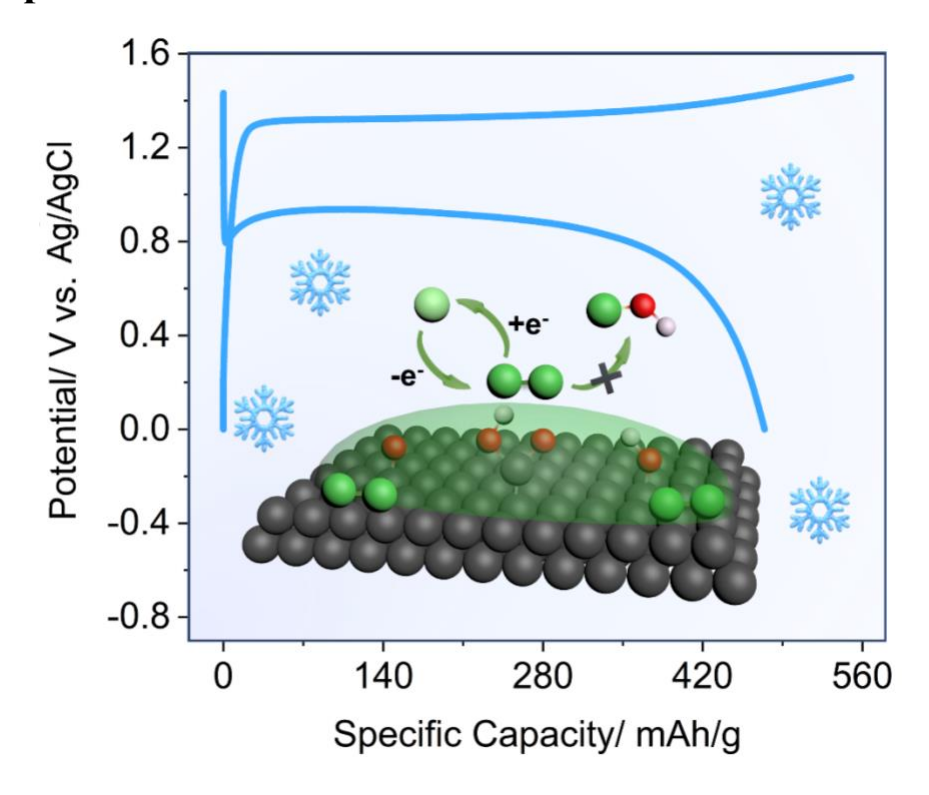
Yiming Sui¹, Ming Lei², Mingliang Yu¹, Alexis Scida¹, Sean K. Sandstrom¹, William Stickle³, Timothy D. O'Larey¹, De-en Jiang²,*, and Xiulei Ji¹,*

- 1. Department of Chemistry, Oregon State University, Corvallis, OR, 97331-4003, United States
- 2. Department of Chemical and Biomolecular Engineering, University, Vanderbilt University, Nashville, Tennessee 37235, United States
- 3. Hewlett-Packard Co., 1000 NE Circle Blvd., Corvallis, OR 97330, United States
- *david.ji@oregonstate.edu, de-en.jiang@vanderbilt.edu

Abstract

Conventional cathodes generally store charges inside solids, and they usually suffer from compromised performance at low temperatures due to the energy barriers for ion transport. Here we report a reversible "plating" reaction of Cl₂ liquid inside nanoporous carbon as a new electrode for low-temperature aqueous batteries. In a 7 *m* LiCl aqueous electrolyte, the activated carbon electrode delivers a high discharge capacity of 475 mAh/g (based on the carbon active mass in the working electrode) at 100 mA/g at –78 °C with a discharging plateau at ca. 0.95 V *vs.* Ag/AgCl, and retains a high capacity of 238 mAh/g at a high current rate of 1 A/g. Furthermore, this electrode system demonstrates stable cycling with ca. 65% capacity retention after 100 cycles at 500 mA/g with an average Coulombic efficiency above 99%. The results provide a new option for high-energy halogen cathodes at low temperatures.

TOC Graphic



Introduction

Rechargeable batteries usually suffer poor performance at low temperatures with low energy density, large polarization, rapid capacity fading, and poor rate capability. However, a tremendous demand exists for high-performing batteries under extremely cold conditions for applications in polar regions and outer space. ¹⁻³ To date, efforts have been overwhelmingly devoted to designing new electrolyte compositions by employing solvents of low freezing points and low polarity ⁴⁻⁶ and additives that induce the formation of solid electrolyte interphase (SEI) / cathode electrolyte interphase (CEI). ^{7,8} Yet, it is well known that low temperatures impose significant difficulty for the transport of ion charge carriers in electrolytes and in solid lattices of electrode materials. ^{3,9} Regarding the cathodes, most attention has been paid to conventional materials operating on the insertion mechanism such as LiFePO4¹⁰, Li(Ni_xMn_yCo_z)O2¹¹, and V₂O₅. ^{12,10,13} To improve the

redox kinetics of these solid-state electrode materials, the community has employed strategies such as particle-size reduction, surface coating, and design of 3D-porous structures. Recently, it has been found that the proton storage can exhibit excellent performance at extremely low temperatures due to its small size and the unique Grotthuss conduction mechanism. Despite the progress, limited capacity remains the bottleneck for electrodes that operate on solid-state redox reactions. Therefore, it is necessary to explore new redox chemistry to meet the demand for low-temperature batteries.

Herein, we report the reversible plating/stripping of Cl₂ molecules inside an activated carbon (AC) host at a low temperature of –78 °C. Plating usually refers to the deposition of metals by reducing solvated metal cations, and it is rarely used for the formation of elemental nonmetals by oxidizing their anions. However, the latter conversion bears the same characteristics of one family of electrochemical reactions—the conversion of ions to their corresponding elemental phase. Therefore, plating is used here to refer to the formation of liquid Cl₂ by oxidizing Cl⁻ ions. This reaction delivers a high capacity of 475 mAh/g at the rate of 100 mA/g, retains a capacity of 238 mAh/g at a high rate of 1 A/g, and demonstrates relatively stable cycling with ca. 65% capacity retention after 100 cycles at 500 mA/g with an average Coulombic efficiency (CE) above 99%. We found that the Cl₂/Cl⁻ redox can be kinetically controlled, where we studied the related control factors.

The studies of Cl₂/Cl⁻ batteries can be dated back to the 19th century. However, batteries using this redox couple generally suffer from low reversibility due to the Cl₂ gas evolution and the disproportionation reaction in electrolytes. Recently, significant progress has been made by Hou *et al.* and Zhu *et al.* in realizing the highly reversible Cl₂/Cl⁻ reactions in non-aqueous electrolytes through strategies, including using a non-reactive solvent of carbon tetrachloride,

solid-salt additives, *i.e.*, NaCl and LiCl in cathodes, and highly porous graphite host. Note that Cl₂ has a boiling temperature of –34 °C at the atmospheric pressure, below which liquid Cl₂ can serve as an active mass for high-capacity energy storage at low temperatures. However, the electrochemical properties of the Cl₂/Cl⁻ plating/stripping reaction at low temperatures have remained underexplored. Herein, we employed 7 *m* aqueous LiCl that remains liquid at –78 °C as the electrolyte (**Figure S1**), which allows the investigation of the reversibility of the Cl₂/Cl⁻ redox couple at low temperatures. Considering that Cl₂ is liquid, it cannot serve as a self-standing electrode; thus, we selected AC as the host to plate Cl₂ inside.

Results and Discussions

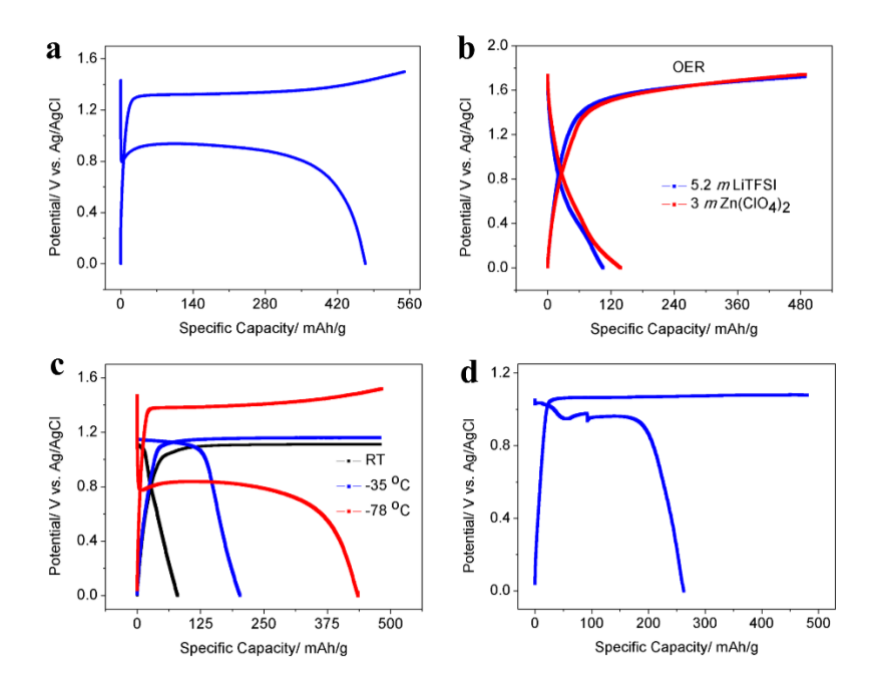


Figure 1. a) GCD profiles of the AC electrode in 7 m LiCl at -78 °C at the current rate of 100 mA/g. b) GCD profiles of the AC electrode in various electrolytes at -35 °C at the rate of 200 mA/g with the same cut-off specific charge capacity of 480 mAh/g. c) GCD profiles of the AC electrode at various temperatures at the rate of 200 mA/g with the same cut-off specific charge

capacity of 480 mAh/g. d) GCD profiles of the AC electrode in 2 m LiCl DMF electrolyte at – 35 °C at the rate of 200 mA/g with the cut-off specific charge capacity of 480 mAh/g.

As shown in **Figure 1a**, the first cycle of the galvanostatic charge-discharge (GCD) test at –78 °C features a discharging capacity of 475 mAh/g and an areal capacity of 1.2 mAh/cm² at a rate of 100 mA/g and the discharging plateau at ca. 0.95 V (vs. Ag/AgCl, hereafter). If the mass of both AC and the engaged LiCl in the electrolyte is considered according to the AC/LiCl stoichiometry corresponding to the capacity, the capacity of the electrode is still at 190 mAh/g. The first cycle exhibits a CE of 86% and a potential hysteresis of 0.4 V, suggesting the excellent reversibility and kinetics of the Cl₂ plating/stripping reaction inside the AC electrode. The half-cell tests were conducted in a three-electrode configuration with the AC free-standing film as a counter electrode, which serves as a sink for counter ions, and Ag/AgCl (1 m HCl) as the reference electrode (**Figures S2** and **S3a**).

What causes the large capacity in the anodic reaction? We tested the AC electrode in two chloridefree control electrolytes at -35 °C, including 5.2 m lithium bis(trifluoromethanesulfonyl)imide (LiTFSI)²¹ and 3 m Zn(ClO4)²² aqueous electrolytes, and one non-aqueous 2 m LiCl in dimethyl formamide (DMF). As shown in **Figure 1b**, neither of the two control aqueous electrolytes presents the plateau behavior as the 7 m LiCl electrolyte does. The results preclude the involvement of water's anodic reaction, *i.e.*, a reversible oxygen evolution reaction and the corrosive Faradaic behavior of the AC electrode as primary capacity sources at low temperatures.²³ Therefore, the reversible capacity featured with one plateau in the GCD profiles originates from the Cl₂/Cl⁻ redox taking place in the AC electrode. In contrast, a well-defined plateau is observed in both 7 m LiCl aqueous electrolyte and 2 m LiCl DMF electrolyte at -35 °C (**Figure 1c, d**). In addition, linear sweep voltammetry (LSV) is carried out at various temperatures for the 7 m LiCl electrolyte with a glassy carbon working electrode (**Figure S3b**). The electrolyte oxidation occurs at 1.35 V, 1.16 V, and 1.1 V (vs the Ag/AgCl (1 m HCl) reference electrode, and hereafter) vs at -78 °C, -35 °C, and RT, respectively, which corroborate the plateau potentials in the GCD tests.

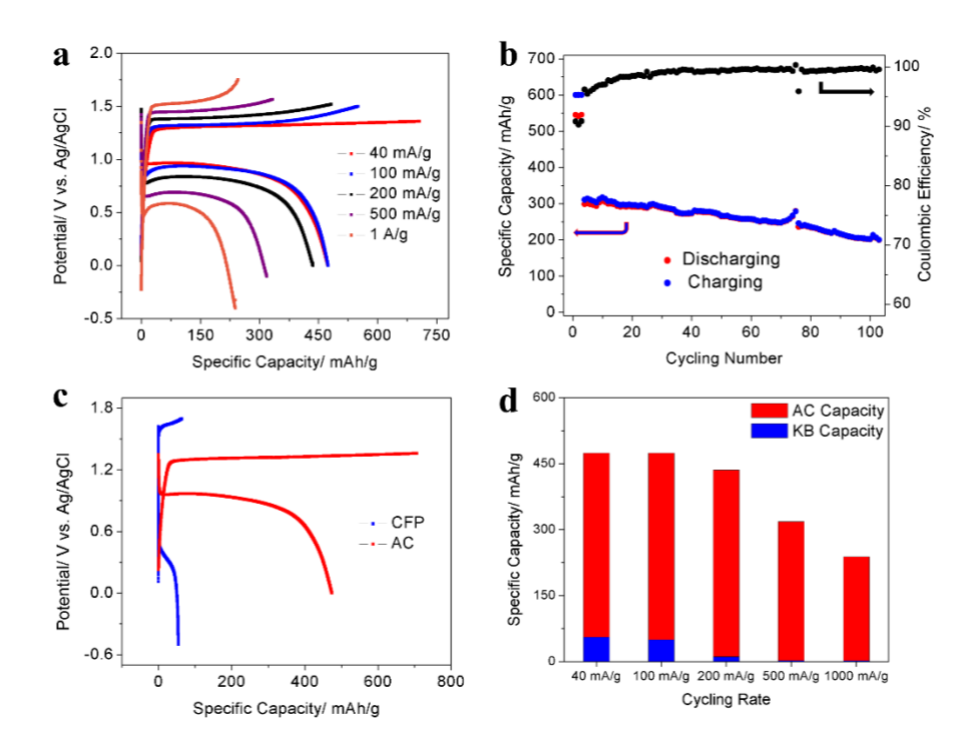


Figure 2. a) GCD profiles of the AC electrode at various rates at −78 °C. b) Cycling performance and CE of AC electrodes at −78 °C at 500 mA/g with the first 3 cycles at 100 mA/g. c) GCD profiles of AC and the CFP electrodes at 40 mA/g and 5 mA/g at −78 °C, respectively. d) Quantitative values of the capacity contribution from active material-AC and conductive additive-KB in electrodes at various rates.

In addition, the Cl₂/Cl⁻ redox reaction over the AC electrode presents excellent rate performance. It delivers high discharging capacities of 474 mAh/g, 474 mAh/g, 435 mAh/g, 318 mAh/g, and 239 mAh/g at current rates of 40 mA/g, 100 mA/g, 200 mA/g, 500 mA/g, and 1A/g, respectively (**Figure 2a**). GCD tests at increased rates demonstrated enhanced CE values from 67% to 86%,

90%, 95%, and 98%, respectively. The AC electrode also shows good cycling stability. When cycling at 500 mA/g, it exhibits 65% capacity retention after 100 cycles with a high average CE of 99% (**Figure 2b**).

Our next question is where the as-formed Cl₂ liquid gets stored. To analyze the capacity contribution from other components besides AC in the electrode, we tested carbon fiber paper (CFP) alone as the electrode and the electrode with KatjenBlack (KB), a conducting carbon additive, bound by polyvinylidene fluoride (PVdF) and coated on CFP in the 7 m LiCl electrolyte at -78 °C. The testing current rates for these cells are calibrated to be the same as the AC electrode (see SI for details). As shown in Figure 2c, the GCD profiles of CFP feature a charging potential at 1.6 V much higher than that of the AC electrodes at 1.3 V; thus, the CFP current collector does not contribute any capacity to the AC electrodes in the testing potential range in Figure 1a. In comparison, KB delivers some capacity of 56 mAh/g and 50 mAh/g, at low cycling rates, i.e., 40 mA/g and 100 mA/g, but offers insignificant capacity at higher rates due to the reaction overpotential (Figure 2d, S4). Therefore, the above results indicate that most plated Cl₂ is stored in the AC and most probably in the nanopores because of the capillary effect. On the other hand, the inclusion of KB as an additive is conducive to the redox kinetics of the AC electrodes by improving the electrical conductivity of the electrode. As shown in Figure S5, EIS results demonstrate that the presence of KB effectively reduces the Ohmic (R_{Ω}) and charge transfer (R_{ct}) resistance from 21 Ω and 76 Ω to 9 Ω and 56 Ω , respectively.

A further question is what electrode properties influence the cycling performance. We collected the GCD results on the AC, graphite, and CFP electrodes at the same rate of 100 mA/g at -78 °C (**Figure 3a**). AC electrodes deliver the highest specific capacity, as well as the lowest reaction polarization, while the CFP electrodes deliver the lowest specific capacity and the largest reaction

polarization. Although many variants exist in the control experiments, the performance differences between the carbon materials shed light on the property-performance correlations.

Scanning electron microscopy (SEM) images show AC and graphite exhibit average particle sizes of 6 μm and 12 μm, respectively, while the CFP is composed of interconnected carbon fibers with a diameter of ca. 8 μm (**Figure S6**). Brunauer–Emmett–Teller (BET) results of the N₂ sorption tests demonstrate that AC exhibits an average pore size of 2.75 nm, a specific pore volume of 1.3 cm³/g, and a high specific surface area of 2440 m²/g, far exceeding that of 30 m²/g for graphite particles and 15 m²/g for CFP (**Figure S7**). Therefore, the amount of stored Cl₂ depends on the porosity of the electrode materials. Furthermore, a rough calculation is conducted to convert the specific capacity of each carbon material to the amount of Cl₂ molecules on the hosts (see **SI** for details), and the results suggest a multi-layer adsorption mechanism for the storage of liquid Cl₂ molecules over the carbon hosts (**Figure S8**, and **Table S1**).

Besides being the host for the liquid Cl₂, the carbon materials serve as the catalysts towards the Cl₂/Cl⁻ redox reaction. The substantial difference in the Cl₂/Cl⁻ redox potentials on different carbon materials indicates their disparate capability of catalyzing the chlorine evolution reaction (CER). As for the structure, AC only exhibits a broad bump at around 20° in its X-ray diffraction (XRD) pattern (**Figure S9**), indicating its non-graphitic structure, while both CFP and graphite present sharp peaks at 26° and 55°, suggesting their highly crystalline graphitic structure. In Raman spectra (**Figure S10**), AC exhibits a high D/G band ratio of 1.02, whereas graphite and CFP demonstrate low D/G band ratios of 0.21 and 0.22, respectively. The results substantiate the fact that AC contains rich structural defects while graphite and CFP are primarily composed of graphitic carbon. X-ray photon spectroscopy (XPS) characterizes the elemental composition and the surface chemical bonding of the carbon materials. Specifically, a higher ratio of oxygen is

found in AC (**Figure S11**). As shown in **Figure 3b** and **3c**, both the high-resolution C 1s and O 1s spectra suggest the existence of C-O, C=O, and -COOH groups on the AC surface. The Fourier transform infrared spectroscopy (FTIR) spectra display the O-H²⁴, C-O^{25,26}, C=O²⁷⁻²⁹, and -COOH²⁸ groups at 3784 cm⁻¹, 1006/2098 cm⁻¹, 1195/ 1720/2332 cm⁻¹, and 1553 cm⁻¹, respectively (**Figure 3d**). In contrast, the surfaces of graphite and GFP are free of functional groups with no peaks observed in their FTIR spectra.

Density functional theory (DFT) calculations were conducted to evaluate the energy barriers for CER on different typical environments: the defect-free basal graphene plane as a model for graphite and defective graphene edge with functional groups as a model for AC (**Figure 3e** and **Figure S12**). At the equilibrium potential of 1.36 V vs. Standard Hydrogen Electrode (SHE), the graphene surface exhibits a Cl* radical adsorption energy (ΔG_{Cl*}) of 0.54 eV. In contrast, the graphene edges with -COOH and -OH species exhibit more favorable Cl adsorption of 0.39 eV and 0.37 eV, respectively, suggesting an eased CER. Interestingly, the graphene edge with the -C=O species shows the lowest ΔG_{Cl*} of -0.75 eV, indicating strong adsorption of Cl* radical and the facilitated CER. In addition, the oxygen-containing moieties withdraw electrons from adjacent carbon atoms, thus making the carbon atoms positively charged as preferable sites for Cl-adsorption (**Figure 3f-i**).

Another factor contributing to the reaction polarization is the surface hydrophilicity of the electrodes. As shown in **Figure S13**, the AC electrode is highly wettable by 7 *m* LiCl with the lowest contact angle of 60° due to the rich hydrophilic groups on the surface. The graphite electrode exhibits a lower contact angle of 97° than the CFP electrode of 120°. The hydrophilic feature of the AC electrode is conducive to the rapid transport of the Cl⁻ anions, thus reducing the polarization of the reaction.

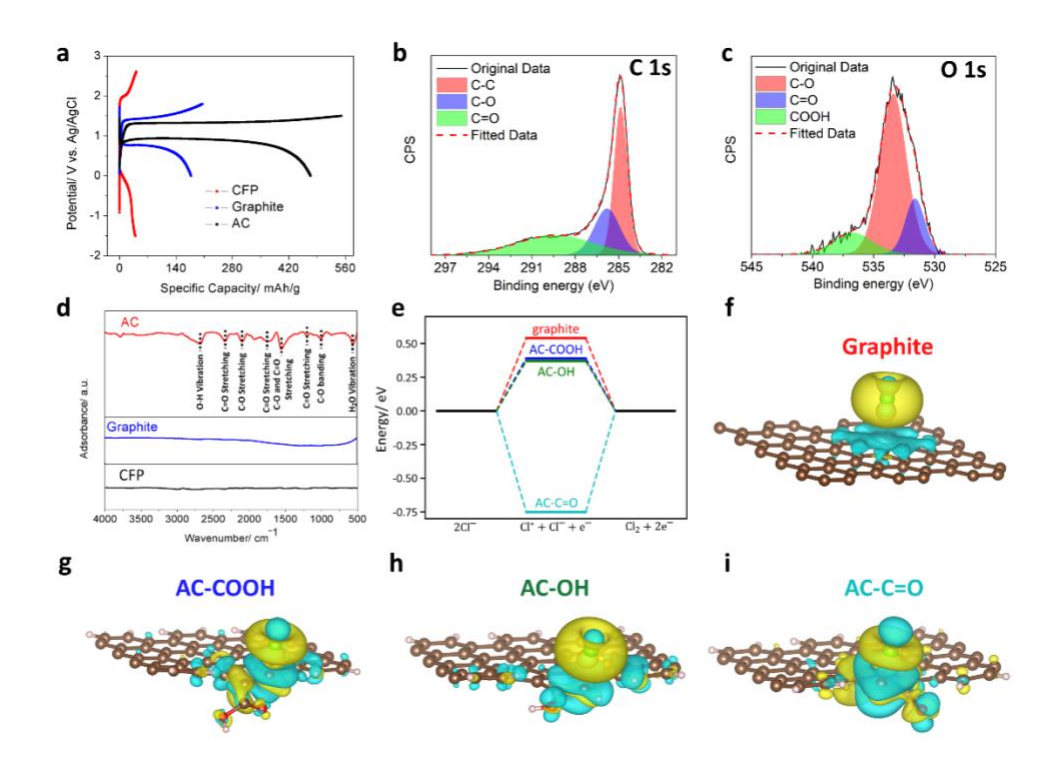


Figure 3. a) GCD profiles of various carbon electrodes at 100 mA/g at –78 °C. High-resolution XPS spectra of b) C 1s and c) O 1s. d) FTIR spectra of various carbon materials. e) DFT calculated energy diagrams of Cl* adsorption over various sites. The charge density difference analysis of f) graphite, g) AC-COOH, h) AC-OH, and i) AC-C=O adsorbed with one Cl⁻. Yellow indicates electron accumulation and blue indicates electron depletion. Brown, green, red, and white balls are carbon, chlorine, oxygen, and hydrogen atoms, respectively.

We deem the low-temperature conditions render the plating of Cl₂ reversibly in the AC electrode via two factors. Firstly, at working temperatures, *i.e.*, -35 °C and -78 °C, the Cl₂ molecules are in the liquid state, which mitigates the Cl₂ gas evolution that causes the loss of active mass. As shown in **Figure S14**, Cl₂ gas bubbles appear at room temperature over the AC electrode during the charging process, which could not be observed at -35 °C. Therefore, the liquid phase of Cl₂ is the

premise of the reversible Cl₂/Cl⁻ redox at low temperatures. Secondly, Cl₂ reacts with water of the electrolyte via a disproportionation reaction, as shown by **Equation 1**:

$$Cl_2 + H_2O \rightarrow HClO + HCl$$
 Equation 1

We postulate that the lower temperatures suppress this side reaction by slowing down the reaction kinetics according to the Arrhenius relationship, thus enhancing the CE values. As a control experiment, we ran the same GCD tests on AC in a 7.5 *m* LiBr aqueous electrolyte at room temperature, where Br₂ is also liquid due to its high boiling point of 58.8 °C (**Figure 4a**). Despite Br₂ exhibits lower reactivity with water than that of Cl₂ because of the lower electronegativity, it presents a lower CE value than that of Cl₂ at –35 °C. The result supports that the suppressed side reaction at low temperatures betters reaction reversibility.

The loss of CE is still closely correlated to the irreversible disproportionation of Cl₂ in electrolytes. For example, the CEs significantly increase with higher cycling rates (**Figure 2a**) and reducing the charging specific capacity from 540 mAh/g to 450 mAh/g and 360 mAh/g is effective in enhancing CE values from 86% to 90% and 93% (**Figure 4b**). In both cases, CEs are improved by shortening the duration when the plated Cl₂ contacts the aqueous electrolyte (**Figure S15**). However, such self-discharge can be self-terminated. After 12-hour of idling at –78 °C, the AC electrode still preserves a discharging capacity of 363 mAh/g, corresponding to a CE of 72.6%, slightly lower than 87.6% for the non-idling electrode (**Figure 4c**). Interestingly, the open circuit potential of the charged AC electrode only drops in the first 1 hour of idling and then keeps constant at ca. 1.1 V, suggesting the existence of a limit for the self-discharging reaction, in other words, the saturation of Cl₂ and HClO in electrolytes (**Figure S16**). The fact may account for the enhanced CE throughout the cycling stability test (**Figure 2b**). Furthermore, in practical cells

where a relatively much smaller volume of the electrolyte is employed, the impact of Cl₂ disproportionation would be smaller.

In addition, we postulate that the capacity fading in the stability test relates to the Cl₂ disproportionation reaction (**Figure 2b**). We first compare the GCD profiles of the AC electrodes at the 10th cycle and 50th cycle, where the latter cycle demonstrated an increased charging (CER) overpotential (**Figure S17**). A higher overpotential reduces the capacity.

As for what causes overpotentials, one hypothesis is that the AC electrode is oxidized by the Cl_2 or HClO during the charging process, which was negated by one control experiment.²⁸ We charged the AC electrode at 200 mA/g for 12 hours in a 7 m LiCl aqueous electrolyte at room temperature (**Figure S18**) before testing this pre-charged electrode again in a pristine 7 m LiCl aqueous electrolyte at -78 °C. The similar GCD profiles between the pristine and the pre-charged electrodes suggest the strong endurance of AC towards the corrosion by Cl_2 or HClO (**Figure 4d**).

On the other hand, the proton generated from the disproportionation reaction of Cl_2 may affect the AC electrode's performance, particularly the overpotential. In another control experiment, we added 0.1 m HCl to 7 m LiCl as the electrolyte, in which the AC electrode exhibits a higher charging overpotential at -78 °C (**Figure 4d**). Evidently, the protons in the electrolyte negatively affect the performance of the AC electrode. Since the disproportionation reaction of Cl_2 in water is spontaneous, the concentration of protons in the electrolyte continuously increases during the cycling process. The question is how protons increase the overpotentials. We attribute this phenomenon to the fact that the functional groups on AC can be protonated in an acidic environment, which eliminates the binding sites, thus, mitigating the catalytic performance (**Figure S19**). $^{30-32}$

As demonstrated in this study, low temperatures may not impose a challenge but provides an excellent opportunity to enable redox-active mass that is gaseous at room temperature. The unique advantages of low temperature batteries are that many gases can be condensed into liquid at low temperatures. Such gases may exhibit intermediate boiling temperatures such as the interhalogen molecules. As for the Cl₂, the side reaction between Cl₂ and water in aqueous electrolytes decreases the CE of the cathode and generates protons to passivate the AC surface. One strategy to enhance performance is to employ nonaqueous electrolytes. Furthermore, Cl₂/Cl⁻ cathode can pair with Li⁺ hosting anode because anion-hosting cathodes allow the usage of a dual-ion battery configuration. The nonaqueous electrolytes with wide electrochemical stability windows allow more anodes with low potentials to pair with Cl₂/Cl⁻ cathode, which opens a new route for designing high-energy batteries at low temperatures.

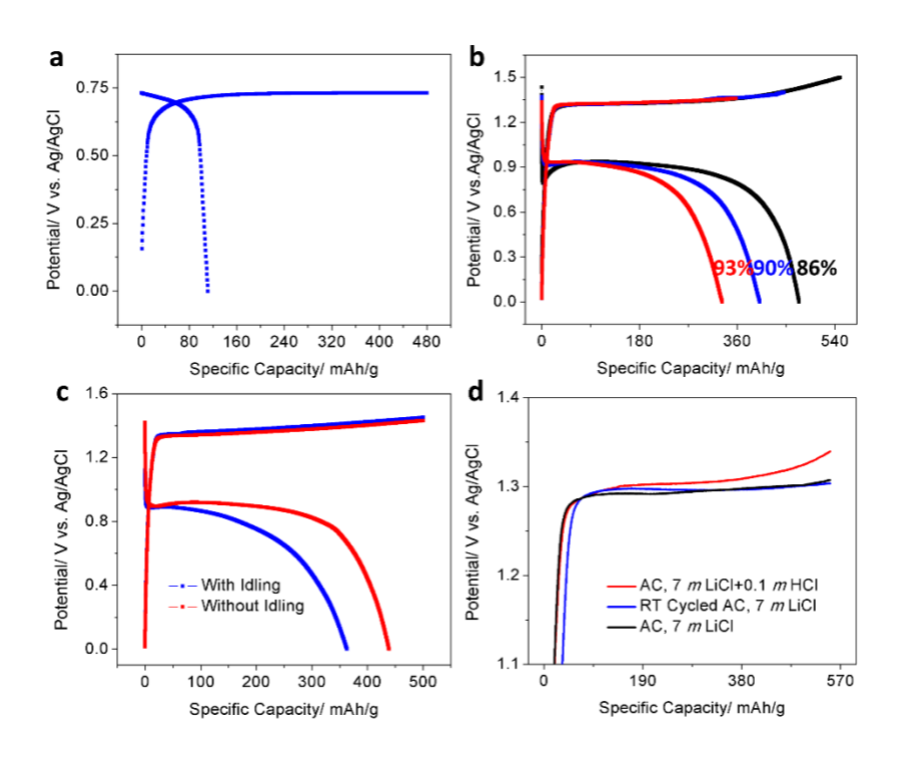


Figure 4. a) GCD profiles of the AC electrode in 7.5 m LiBr at room temperature at the rate of 200 mA/g with the cut-off specific charge capacity of 480 mAh/g. b) GCD profiles of AC electrode

at various specific charging capacities at 100 mA/g. c) GCD profiles of AC electrode with (red) and without (blue) 12-hour idling between the charging and discharging process at 100 mA/g with the same charging capacity of 500 mAh/g. d) Charging profiles of the pristine AC electrode tested in 7 m LiCl and 7 m LiCl + 0.1 m HCl aqueous electrolytes and RT cycled AC tested in 7 m LiCl aqueous electrolyte at 100 mA/g at -78 °C with the same cut-off specific charge capacity of 550 mAh/g.

Conclusions

In summary, we investigated the reversible Cl₂/Cl⁻ redox reaction by using an AC electrode and 7 *m* LiCl aqueous electrolyte at –78 °C. The electrode delivers a high discharging capacity of 475 mAh/g at discharging potential at ca. 0.95 V *vs.* Ag/AgCl at 100 mA/g as well as good rate capability and stable cycling performance. The low-temperature conditions play a critical role in stabilizing the charging product: Cl₂ molecules in its liquid phase. Furthermore, the low temperature suppresses the disproportionation reaction of Cl₂ molecules in the aqueous electrolyte. In addition, AC electrode serves both the catalyst for the reaction and the host for the Cl₂ molecules. The work opens a new route for designing high-energy battery electrodes at extremely low temperatures.

Acknowledgments

X. J. and D. J. thank the U.S. National Science Foundation (NSF) for the financial support with the Awards DMR 2221645 and DMR 2221646.

References

(1) Sui, Y.; Yu, M.; Xu, Y.; Ji, X. Low-Temperature Aqueous Batteries: Challenges and Opportunities. *J. Electrochem. Soc.* **2022**, *169* (3), 030537.

- Jow, T. R.; Delp, S. A.; Allen, J. L.; Jones, J.-P.; Smart, M. C. Factors Limiting Li⁺ Charge Transfer Kinetics in Li-lon Batteries. *J. Electrochem. Soc.* **2018**, *165* (2), A361.
- (3) Gupta, A.; Manthiram, A. Designing Advanced Lithium-Based Batteries for Low-Temperature Conditions. *Adv. Energy Mater.* **2020,** *10* (38), 2001972.
- (4) Nan, B.; Chen, L.; Rodrigo, N. D.; Borodin, O.; Piao, N.; Xia, J.; Pollard, T.; Hou, S.; Zhang, J.; Ji, X.et al. Enhancing Li⁺ Transport in NMC811||Graphite Lithium-Ion Batteries at Low temperatures by Using Low-Polarity-Solvent Electrolytes. *Angew. Chem. Int. Ed.* **2022**, *134*, e202205967.
- (5) Holoubek, J.; Liu, H.; Wu, Z.; Yin, Y.; Xing, X.; Cai, G.; Yu, S.; Zhou, H.; Pascal, T. A.; Chen, Z.et al. Tailoring Electrolyte Solvation for Li Metal Batteries Cycled at Ultra-Low Temperature. *Nat. Energy* **2021**, *6* (3), 303-313.
- (6) Rustomji, C. S.; Yang, Y.; Kim, T. K.; Mac, J.; Kim, Y. J.; Caldwell, E.; Chung, H.; Meng, Y. S. Liquefied Gas Electrolytes for Electrochemical Energy Storage Devices. *Science* **2017**, *356* (6345), eaal4263.
- (7) Fan, X.; Ji, X.; Chen, L.; Chen, J.; Deng, T.; Han, F.; Yue, J.; Piao, N.; Wang, R.; Zhou, X.et al. All-Temperature Batteries Enabled by Fluorinated Electrolytes with Non-Polar Solvents. *Nat. Energy* **2019**, *4* (10), 882-890.
- (8) Thenuwara, A. C.; Shetty, P. P.; Kondekar, N.; Sandoval, S. E.; Cavallaro, K.; May, R.; Yang, C.-T.; Marbella, L. E.; Qi, Y.; McDowell, M. T. Efficient Low-Temperature Cycling of Lithium Metal Anodes by Tailoring the Solid-Electrolyte Interphase. *ACS Energy Lett.* **2020**, *5* (7), 2411-2420.
- (9) Zhang, S. S.; Xu, K.; Jow, T. R. The Low Temperature Performance of Li-Ion Batteries. *J. Power Sources* **2003**, *115* (1), 137-140.
- (10) Wu, X.-L.; Guo, Y.-G.; Su, J.; Xiong, J.-W.; Zhang, Y.-L.; Wan, L.-J. Carbon-Nanotube-Decorated Nano-LiFePO₄ @C Cathode Material with Superior High-Rate and Low-Temperature Performances for Lithium-Ion Batteries. *Adv. Energy Mater.* **2013**, *3* (9), 1155-1160.
- (11) Li, Q.; Lu, D.; Zheng, J.; Jiao, S.; Luo, L.; Wang, C.-M.; Xu, K.; Zhang, J.-G.; Xu, W. Li⁺-Desolvation Dictating Lithium-Ion Battery's Low-Temperature Performances. *ACS Appl. Mater. Interfaces* **2017**, *9* (49), 42761-42768.
- (12) Zhang, Q.; Xia, K.; Ma, Y.; Lu, Y.; Li, L.; Liang, J.; Chou, S.; Chen, J. Chaotropic Anion and Fast-Kinetics Cathode Enabling Low-Temperature Aqueous Zn Batteries. *ACS Energy Lett.* **2021**, *6* (8), 2704-2712.
- (13) Zhang, N.; Deng, T.; Zhang, S.; Wang, C.; Chen, L.; Wang, C.; Fan, X. Critical Review on Low-Temperature Li-Ion/Metal Batteries. *Adv. Mater.* **2022**, *34* (15), 2107899.
- Jiang, H.; Shin, W.; Ma, L.; Hong, J. J.; Wei, Z.; Liu, Y.; Zhang, S.; Wu, X.; Xu, Y.; Guo, Q.et al. A High-Rate Aqueous Proton Battery Delivering Power Below –78 °C via an Unfrozen Phosphoric Acid. *Adv. Energy Mater.* **2020**, *10* (28), 2000968.
- Zhu, Z.; Wang, W.; Yin, Y.; Meng, Y.; Liu, Z.; Jiang, T.; Peng, Q.; Sun, J.; Chen, W. An Ultrafast and Ultra-Low-Temperature Hydrogen Gas—Proton Battery. *J. Am. Chem. Soc.* **2021**, *143* (48), 20302-20308
- (16) Winter, L. a. G. D. Minute Epics of Flight: Grosset & Dunlap, 1933.
- (17) Thomas, D. L.; Bennion, D. N. A LiAl /Cl₂ Battery with a Four-Component Alkali-Metal Chloride Electrolyte. *J. Electrochem. Soc.* **1989**, *136* (12), 3553.
- (18) Klinedinst, K. A.; Domeniconi, M. J. High Rate Discharge Characteristics of Li / SOCl₂ Cells. *J. Electrochem. Soc.* **1980**, *127* (3), 539.
- (19) Hou, S.; Chen, L.; Fan, X.; Fan, X.; Ji, X.; Wang, B.; Cui, C.; Chen, J.; Yang, C.; Wang, W.et al. High-Energy and Low-Cost Membrane-Free Chlorine Flow Battery. *Nat. Commun.* **2022**, *13* (1), 1281.
- (20) Zhu, G.; Tian, X.; Tai, H.-C.; Li, Y.-Y.; Li, J.; Sun, H.; Liang, P.; Angell, M.; Huang, C.-L.; Ku, C.-S.et al. Rechargeable Na/Cl₂ and Li/Cl₂ batteries. *Nature* **2021**, *596* (7873), 525-530.

- (21) Kim, H.-I.; Shin, E.; Kim, S.-H.; Lee, K. M.; Park, J.; Kang, S. J.; So, S.; Roh, K. C.; Kwak, S. K.; Lee, S.-Y. Aqueous Eutectic Lithium-Ion Electrolytes for Wide-Temperature Operation. *Energy Storage Mater.* **2021**, *36*, 222-228.
- Yang, G.; Huang, J.; Wan, X.; Liu, B.; Zhu, Y.; Wang, J.; Fontaine, O.; Luo, S.; Hiralal, P.; Guo, Y.et al. An Aqueous Zinc-Ion Battery Working at -50°C Enabled by Low-Concentration Perchlorate-Based Chaotropic Salt Electrolyte. *EcoMat* **2022**, *4* (2), e12165.
- (23) Qu, D.; Shi, H. Studies of Activated Carbons Used in Double-Layer Capacitors. *J. Power Sources* **1998**, *74* (1), 99-107.
- (24) Barroso-Bogeat, A.; Alexandre-Franco, M.; Fernández-González, C.; Gómez-Serrano, V. FT-IR Analysis of Pyrone and Chromene Structures in Activated Carbon. *Energy Fuels* **2014**, *28* (6), 4096-4103.
- (25) Mueller, B.; van Langeveld, A. D.; Moulijn, J. A.; Knoezinger, H. Characterization of Sulfided Molybdenum/Alumina Catalysts by Temperature-Programmed Reduction and Low-Temperature Fourier Transform Infrared Spectroscopy of Adsorbed Carbon Monoxide. J. Phys. Chem. 1993, 97 (35), 9028-9033.
- (26) Hoseinzadeh Hesas, R.; Arami-Niya, A.; Wan Daud, W. M. A.; Sahu, J. N. Comparison of Oil Palm Shell-Based Activated Carbons Produced by Microwave and Conventional Heating Methods Using Zinc Chloride Activation. *J. Anal. Appl. Pyrolysis.* **2013**, *104*, 176-184.
- (27) Wu, T.-M.; Lin, Y.-W.; Liao, C.-S. Preparation and Characterization of Polyaniline/Multi-Walled Carbon Nanotube Composites. *Carbon* **2005**, *43* (4), 734-740.
- (28) El-Hendawy, A.-N. A. Influence of HNO₃ Oxidation on the Structure and Adsorptive Properties of Corncob-Based Activated Carbon. *Carbon* **2003**, *41* (4), 713-722.
- (29) Gaya, U. I.; Otene, E.; Abdullah, A. H. Adsorption of Aqueous Cd(II) and Pb(II) on Activated Carbon Nanopores Prepared by Chemical Activation of Doum Palm Shell. *SpringerPlus* **2015**, *4* (1), 458.
- (30) Cristiano, E.; Hu, Y.-J.; Siegfried, M.; Kaplan, D.; Nitsche, H. A Comparison of Point of Zero Charge Measurement Methodology. *Clays Clay Miner.* **2011**, *59* (2), 107-115.
- (31) Stewart, R.; Yates, K. The Protonation of the Carbonyl Group. I. The Basicity of Substituted Acetophenones1. *J. Am. Chem. Soc.* **1958**, *80* (23), 6355-6359.
- (32) Stewart, R.; Yates, K. The Position of Protonation of the Carboxyl Group¹. *J. Am. Chem. Soc.* **1960**, 82 (15), 4059-4061.